Chinese Chemical Letters 37 (2026) 111820

Contents lists available at ScienceDirect

Chinese Chemical Letters

journal homepage: www.elsevier.com/locate/cclet

Electronic interactions and hydrogen migration over C_{60}-modified Ru catalyst enhance ammonia synthesis

Xuanbei Peng[a,b,1], Xiaohu Hu[c,1], Ruishao Mao[b,1], Mengqi An[b], Jiaxin Li[b], Yangyu Zhang[b], Tianhua Zhang[b], Ming Chen[b], Yanliang Zhou[a,b], Jun Ni[b,*], Lirong Zheng[d], Xiuyun Wang[a,b,*], Lilong Jiang[a,b,*]

[a] Qingyuan Innovation Laboratory, Quanzhou 362801, China
[b] National Engineering Research Center of Chemical Fertilizer Catalyst, Fuzhou University, Fuzhou 350002, China
[c] Institute of Molecular Plus, Department of Chemistry, School of Chemical Engineering and Technology, Tianjin University, Tianjin 300072, China
[d] Institute of High Energy Physics, Chinese Academy of Sciences, Beijing 100049, China

ARTICLE INFO

Article history:
Received 20 May 2025
Revised 23 August 2025
Accepted 10 September 2025
Available online 10 September 2025

Keywords:
N_2 activation
Carbon clusters
Ru catalysts
Hydrogen spillover
NH_3 desorption

ABSTRACT

The potential use of ammonia (NH_3) as a hydrogen energy carrier has generated significant interest in developing efficient catalysts for producing NH_3 under mild conditions. The main obstacles for NH_3 synthesis are the activation of the N≡N bond and the desorption of NH_3 from the catalyst surface. Here, we report the use of C_{60} to overcome these challenges. Through electron transfer, migration, and feedback between C_{60} and Ru, there is a balance of electronic density at the Ru active sites and a shift in the d-band center. This simultaneously satisfies the electronic requirements for enhancing N_2 activation while weakening NH_3 adsorption, thereby circumventing the bottlenecks in NH_3 synthesis under mild conditions. Meanwhile, anchoring of C_{60} accelerates hydrogen spillover and enhances the exchangeability of hydrogen species in the ZrH_2 support, as well as expose a greater number of B_5 sites of Ru entities, resulting in the co-optimization of hydrogen migration and nitrogen activation. As a consequence, the NH_3 synthesis rate of the C_{60}-Ru/ZrH_2 catalyst is approximately twice that of the Ru/ZrH_2 catalyst at 400 °C and 1 MPa. This study shows that doping C_{60} represents a fundamentally different approach compared to traditional promoters for catalytic NH_3 synthesis. We anticipate that this strategy may be generalized to generate widespread interest in the catalysis of NH_3 synthesis.

© 2026 Published by Elsevier B.V. on behalf of Chinese Chemical Society and Institute of Materia Medica, Chinese Academy of Medical Sciences.

Ammonia (NH_3) is a major nitrogen source for the production of fertilizers and other nitrogen-containing chemicals [1,2]. Furthermore, it is also increasingly recognized as an alternative hydrogen energy vector [3–5]. The current industrial NH_3 production heavily relies on the well-established Haber-Bosch (H-B) process using iron-based catalyst, which requires high temperatures and pressures (400−500 °C, 10−30 MPa) [6–8]. Additionally, the supply of hydrogen (H_2) primarily comes from the steam reforming of natural gas or coal accompanying by high energy consumption, accounting for 1%−2% of the global energy supply and at least 500 million tons of greenhouse gas emissions per year [1,9,10]. Therefore, under the background of energy conservation and carbon neutrality, it is essential to develop an energy-saving and environmentally friendly NH_3 synthesis process [11]. Currently, the technology for producing H_2 *via* water electrolysis using renewable energy is becoming increasingly mature. Coupling water electrolysis with the H-B process for NH_3 synthesis can significantly reduce energy consumption and carbon emissions [12,13]. To achieve this, the development advanced catalysts that can produce NH_3 efficiently under mild conditions is crucial for NH_3 synthesis.

It is well known that the NH_3 synthesis reaction consists of several key steps, such as the activation of the reaction molecules N_2 and H_2, the formation of the intermediate NH_x species and the desorption of NH_3 [14]. Among them, the dissociation of N_2 is generally considered to be the rate-determining step (RDS) for NH_3 synthesis. Therefore, extensive efforts have been dedicated to the development of novel catalysts aimed at investigating N_2 activation pathways to reduce the reaction energy barrier. In recent years, various types of support materials, including electride materials [15], nitrides [16–18], hydrides [19,20], perovskite oxynitride-

* Corresponding authors at: National Engineering Research Center of Chemical Fertilizer Catalyst, Fuzhou University, Fuzhou 350002, China.
E-mail addresses: nj@fzu.edu.cn (J. Ni), xywangfzu@163.com (X. Wang), jll@fzu.edu.cn (L. Jiang).
[1] These authors contributed equally to this work.

https://doi.org/10.1016/j.cclet.2025.111820
1001-8417/© 2026 Published by Elsevier B.V. on behalf of Chinese Chemical Society and Institute of Materia Medica, Chinese Academy of Medical Sciences.

hydrides [21], and intermetallic compounds [22], supported transition metal catalysts have been reported to exhibit excellent catalytic activities for NH_3 synthesis under mild conditions. Compared to oxide supports, these hydrides and nitrides provide advantages in NH_3 synthesis due to their anion vacancies, which facilitate the activation or reaction with N_2. For example, Zhou *et al.* [23] investigated the impact of metal-anion interactions on NH_3 synthesis performance in different Zr materials (*i.e.*, ZrH_2, ZrN, and ZrO_2)-supported Ru catalysts. The results indicated that the moderate Ru-H interaction and easy hydrogen spillover in ZrH_2, which facilitates the activation of N_2 at the Ru sites. In addition to modifying the support composition, promoters also play a crucial role in enhancing the catalytic activity of metal catalysts. In the absence of electronic promoters, even industrially utilized Ru or Fe-based catalysts exhibit negligible catalytic performance [24,25]. At present, the promoters that are extensively studied in NH_3 synthesis primarily include alkali metals, alkaline earth metals, and rare earth elements [26]. These element promoters facilitate unidirectional electron transfer to the surfaces of active metals, thereby increasing their electron density and enhancing catalytic performance. Unlike elemental promoters, fullerene C_{60} has been reported to function as an "electron buffer" in metal-based catalysts, which can dynamically store and release electrons, thereby helping to balance the electron density of active metal species [27,28]. Additionally, the C_{60} possesses a unique geometric structure and the ability to reversibly store and release hydrogen, which leads to the development of C_{60}-modified, oxide-supported Ru-based catalysts that mitigate the effects of hydrogen poisoning [28]. Anchoring a controllable C_{60} layer on Mo_2CT_x as a second H_2 adsorption site enhances their electronic interaction, substantially improving NH_3 synthesis performance [29]. These unique properties enable C_{60} to overcome the limitations of traditional element promoters and therefore exhibit potential for NH_3 synthesis under mild conditions.

Herein, C_{60}-modified Ru/ZrH_2 catalysts were prepared by a straightforward solvent-free ball milling method. Experimental characterizations demonstrate that the introduction of C_{60} decreases the size and increases the dispersion of Ru species, leading to the formation of more B_5 active sites, which is beneficial to the activation of N_2. Meanwhile, the interaction between Ru and C_{60} results in a significant decrease in the work function and an increase in the electron density of Ru atoms, as well as induces a shift in the d-band center. This promotes the activation of N_2 and the desorption of produced NH_3. Moreover, the presence of C_{60} promotes the migration of hydrogen atoms and accelerates the exchange of hydrogen species in ZrH_2 with gaseous H_2. Therefore, the C_{60}-modified Ru/ZrH_2 catalyst shows a higher NH_3 synthesis rate than free-C_{60} sample. Our findings could stimulate broad interest in using C_{60} for NH_3 synthesis under mild conditions.

Initially, pristine C_{60} was investigated for NH_3 synthesis, and the corresponding result is depicted in Fig. 1a. At 400 °C and 1 MPa, pristine C_{60} exhibits inactivity, resulting in a negligible rate of NH_3 synthesis. Meanwhile, the NH_3 synthesis rate of pure ZrH_2 is only 0.1 $mmol_{NH3}$ g_{cat}^{-1} h^{-1}. Anchoring Ru onto ZrH_2 support (Table S1 in Supporting information) increases the NH_3 synthesis rate to 6.4 $mmol_{NH3}$ g_{cat}^{-1} h^{-1}. Further anchoring C_{60} onto Ru/ZrH_2 results in an NH_3 synthesis rate of 12.5 $mmol_{NH3}$ g_{cat}^{-1} h^{-1}, which is about ~2 times as high as that of the Ru/ZrH_2 catalyst (Fig. 1a). Moreover, a volcano-type dependence between N_2/H_2 vol ratio and NH_3 synthesis rate over C_{60}-Ru/ZrH_2 is observed, exhibiting the maximum of 15.6 $mmol_{NH3}$ g_{cat}^{-1} h^{-1} at ~1/1 (Fig. S1 in Supporting information). To evaluate the intrinsic activity of Ru/ZrH_2 and C_{60}-Ru/ZrH_2 catalysts, the total turnover frequency ($TOF_{Ru\ total}$) and the surface turnover frequency ($TOF_{Ru\ surface}$) were calculated based on the total and surface Ru atom counts, respectively. Remarkably, the $TOF_{Ru\ total}$ and $TOF_{Ru\ surface}$ of C_{60}-Ru/ZrH_2 reach values as high as

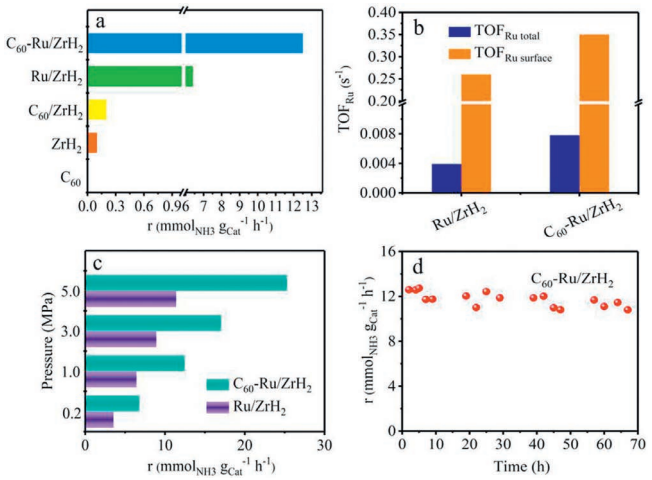


Fig. 1. (a) NH_3 synthesis rate and (b) TOF_{Ru} of Ru/ZrH_2 catalysts with or without C_{60} promotion. (c) Dependence of NH_3 synthesis rate on the reaction pressure at 400 °C for Ru/ZrH_2 catalysts with or without C_{60} promotion. (d) Catalytic stability of C_{60}-mediated Ru/ZrH_2 catalyst (conditions: N_2:H_2 = 1:3; 400 °C and 1 MPa).

7.80×10^{-3} and 0.35 s^{-1} at 400 °C and 1 MPa (Fig. 1b), respectively. These values are significantly higher than those of Ru/ZrH_2, highlighting the crucial role of C_{60} in enhancing intrinsic activity.

Fig. 1c displays the variation in the NH_3 synthesis rate as a function of reaction pressure for both Ru/ZrH_2 and C_{60}-Ru/ZrH_2 at 400 °C. Clearly, the NH_3 synthesis rate over Ru/ZrH_2 and C_{60}-Ru/ZrH_2 exhibits an approximately linear increase with pressure rises from 0.2 MPa to 5.0 MPa, implying that utilizing ZrH_2 hydride as a support can mitigate the hydrogen poisoning effect caused by strong hydrogen absorption on Ru-based catalysts. Stability is a crucial factor for evaluating the catalytic activity of the C_{60}-promoted Ru/ZrH_2 catalyst in NH_3 synthesis. No significant deactivation of the NH_3 synthesis rate was observed during continuous operation for 67 h at 400 °C and 1 MPa (Fig. 1d), confirming the long-term stability of the C_{60}-Ru/ZrH_2 catalyst. Moreover, the concentration of methane discerned in the exhaust is negligible and quite low (Fig. S2 in Supporting information), indicating that C_{60} is stable under the adopted conditions for NH_3 synthesis. Additionally, high-performance liquid chromatography-atmospheric pressure chemical ionization-mass spectrometry (HPLC-APCI-MS) analysis of the used C_{60}-Ru/ZrH_2 catalyst shows a sharp peak located at ~720 *m/z* (Fig. S3 in Supporting information), which is attributed to the C_{60} molecule [30]. Notably, most of the C_{60} in the used C_{60}-Ru/ZrH_2 sample can be recovered after the reaction through the condensation reflux of the toluene solution. Subsequent XRD analysis further confirms that the structure of the recycled C_{60} is similar to that of the fresh sample (Fig. S4 in Supporting information). All these observations indicate that the C_{60}-modified Ru/ZrH_2 sample is highly active and stable under the adopted NH_3 synthesis conditions.

To gain the mechanism information for NH_3 synthesis, kinetic analyses were conducted over Ru/ZrH_2 and C_{60}-Ru/ZrH_2. The apparent activation energy (E_a) of the Ru/ZrH_2 catalyst is estimated to be 84 kJ/mol (Fig. 2a), which decreases to 68 kJ/mol after the addition of C_{60}. Such low E_a value for the C_{60}-Ru/ZrH_2 catalyst is significantly lower than that of conventional Ru-based catalysts (90–120 kJ/mol, Table S2 in Supporting information). These observations reveal that the introduction of C_{60} could decrease the reaction barrier for NH_3 synthesis. The N_2 reaction order (α) of the C_{60}-Ru/ZrH_2 catalyst is 0.79 (Fig. 2b), which is remarkably lower than that of the Ru/ZrH_2 (1.36), proving that the addition of C_{60} can promote the adsorption and activation of N_2 [31]. The distinct differences in the α value observed between the Ru/ZrH_2 and C_{60}-

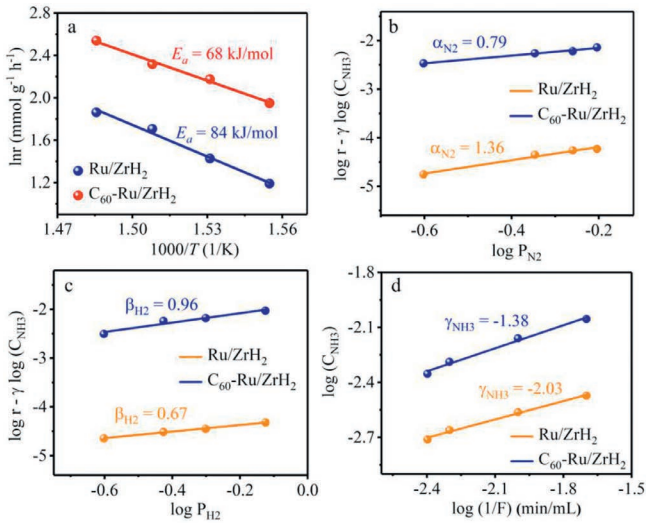


Fig. 2. (a) Arrhenius plot of Ru/ZrH_2 and C_{60}-Ru/ZrH_2 at 1 MPa. Reaction orders of (b) N_2, (c) H_2, and (d) NH_3 over the Ru/ZrH_2 and C_{60}-Ru/ZrH_2 at 400 °C and 1 MPa.

Ru/ZrH_2 catalysts can be ascribed to the variation of the size and electronic structure of the Ru entities after C_{60} doping (*vide infra*). Interestingly, both Ru/ZrH_2 and C_{60}-Ru/ZrH_2 catalysts exhibit a positive reaction order with respect to H_2 (Fig. 2c). This observation suggests that the ZrH_2 support effectively avoids hydrogen poisoning effect on Ru catalysts [32], which are consistent with the finding that the NH_3 synthesis rate increases monotonically with reaction pressure (Fig. 1c). The absence of hydrogen poisoning effect may result from ZrH_2 is a strong electron-donating support material that has reversible hydrogen storage-and-release ability [33,34].

Moreover, the reaction order of NH_3 over Ru/ZrH_2 is −2.03 (Fig. 2d), implying that the adsorbed NH_x species are too strong to desorb from the catalyst surface at low temperature, resulting in the requirement for high temperature to desorb the adsorbed NH_3 [16,35]. The addition of C_{60} to the Ru/ZrH_2 catalyst results in the increase of the NH_3 reaction order to −1.38, indicating that C_{60} induces weak adsorption of NH_3 on the catalyst surface, possibly due to its electronic effect (*vide infra*). Overall, these kinetic analyses indicate that the introduction of C_{60} could simultaneously enhance the activation of N_2 and weaken the adsorption of the product NH_3 on the catalyst surface.

To elucidate the impact of C_{60} on the chemical state over the Ru/ZrH_2, the physicochemical properties of Ru/ZrH_2 and C_{60}-Ru/ZrH_2 were investigated. X-ray diffraction (XRD) was used to analyze the crystal structure of the prepared catalysts. As shown in Fig. S5a (Supporting information), the XRD patterns of the Ru/ZrH_2 and C_{60}-Ru/ZrH_2 mainly show the characteristic diffraction peak of ZrH_2 (JCPDS No. 073–2076). Two additional diffraction peaks at 38.38° and 44.02° for the Ru/ZrH_2 catalyst are attributed to the hexagonal Ru (100) and (101) crystal planes (JCPDS No. 089–4903) (Fig. S5b in Supporting information). However, the diffraction peaks related to Ru species disappear after the doping of C_{60}, indicating that the addition of C_{60} decreases the size and promotes the dispersion of Ru species. Moreover, no diffraction peaks related to C_{60} are observed, primarily due to the high dispersion of C_{60} on the support or because the size of the C_{60} layer falls below the detection limit of the XRD technique. Besides, the ^{13}C-labeled solid-state nuclear magnetic resonance (ssNMR) spectrum of the C_{60}-Ru/ZrH_2 shows a peak at 143.8 ppm, corresponding to the characteristics of underivatized C_{60} with I_h symmetry [36,37], indicating that C_{60} has been successfully loaded onto the catalyst (Fig. S6 in Supporting information).

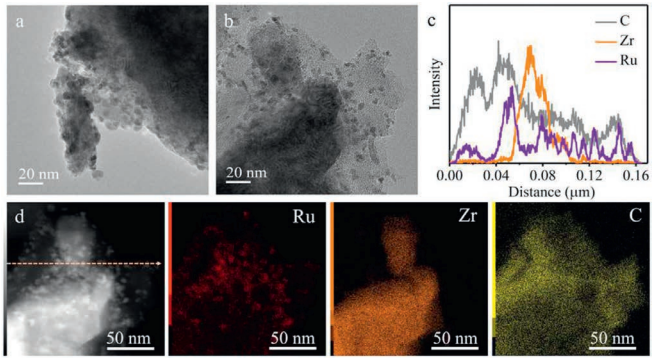


Fig. 3. TEM images and the corresponding Ru particle size distributions of (a) Ru/ZrH_2 and (b) C_{60}-Ru/ZrH_2. (c) Line scan profiles of C_{60}-Ru/ZrH_2 corresponding to the position in picture d. (d) HAADF–STEM image of C_{60}-Ru/ZrH_2 and related EDX mappings of Ru, Zr and C elements.

Raman spectrum of pure C_{60} shows three distinct bands at 267, 493 and 1457 cm^{-1}, which are attributed to the $A_g(1)$, $H_g(1)$ and $A_g(2)$ vibrational modes of the fullerene C_{60} [38], respectively (Fig. S7a in Supporting information). All of the Raman bands of C_{60} are also observed in the case of C_{60}-Ru/ZrH_2, proving that C_{60} has been successfully incorporated into the Ru/ZrH_2 catalyst. Notably, the position of the $A_g(2)$ peak is an important index of the charge transfer between C_{60} and transition metals [39,40]. Compared to pure C_{60} (1457 cm^{-1}), the $A_g(2)$ peak of C_{60}-Ru/ZrH_2 shifts to 1462 cm^{-1} (Fig. S7b in Supporting information), implying that the existence of a strong electronic interaction between Ru atom and C_{60} clusters. The specific surface area of Ru/ZrH_2 is 5.8 m^2/g, which increases to 33.8 m^2/g for C_{60}-Ru/ZrH_2 (Table S1 in Supporting information). The increase of the specific surface area can be attributed to the addition of C_{60}, which improves the pore structure of the catalyst.

Transmission electron microscopy (TEM, Fig. 3a) and high-angle annular dark-field scanning-TEM (HAADF-STEM, Figs. S8a-c in Supporting information) images of the Ru/ZrH_2 catalyst reveal the presence of large agglomerated Ru nanoparticles, with an average particle size of ~6.5 nm on the ZrH_2 support. Interestingly, the addition of C_{60} leads to a decrease in the size of Ru, resulting in a uniform size of approximately 3.6 nm (Fig. 3b and Figs. S8d-f in Supporting information). This observation further indicates that the introduction of C_{60} facilitates the dispersion of the Ru nanoparticles, as confirmed by the results of the CO pulse experiment (Table S1). The TEM images of Ru/ZrH_2 and C_{60}-Ru/ZrH_2 primarily display two distinct lattice fringes with spacings of 0.21 and 0.28 nm (Figs. S9 and S10 in Supporting information), corresponding to the (101) crystal plane of metallic Ru and (101) crystal plane of ZrH_2 [41,42], respectively. Notably, the line scan profiles of C_{60}-Ru/ZrH_2 display that C_{60} layers are wrapped around the periphery of the Ru/ZrH_2 (Fig. 3c). Such continuous carbon shells could accelerate the charge transport [43]. Besides, the energy-dispersive X-ray spectroscopy (EDX) mappings of C_{60}-Ru/ZrH_2 reveal the relatively homogeneous dispersion of Ru, Zr, and C elements throughout the catalyst (Fig. 3d).

Previous studies have shown that the amount of exposed surface-active sites, such as B_5 sites, gradually increases as the size of Ru particles decreases [44–46]. Compared to Ru/ZrH_2, C_{60}-Ru/ZrH_2 exhibits a smaller Ru particle size, suggesting that more active sites are available for N_2 activation. To investigate the effect of C_{60} on Ru adsorption sites, *in situ* diffuse reflectance infrared Fourier transform spectroscopic (DRIFTS) measurement using CO as a probe over Ru/ZrH_2 and C_{60}-Ru/ZrH_2 was performed. As shown in Fig. 4a, in addition to the two gaseous CO adsorption peaks at 2175 and 2115 cm^{-1}, a shoulder peak at 2066 cm^{-1} observed over

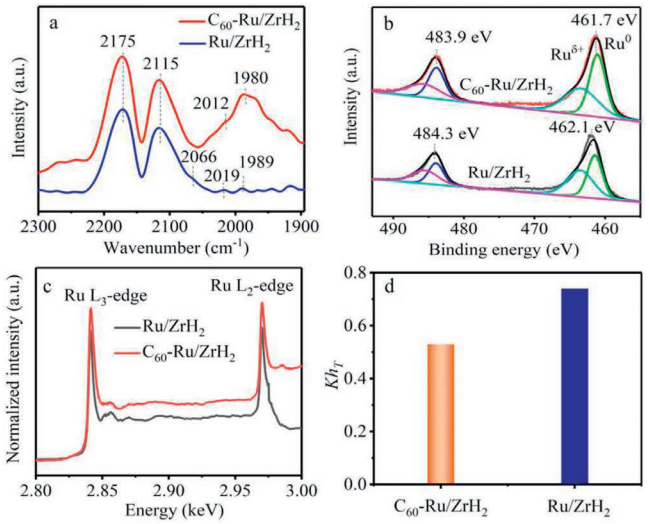


Fig. 4. (a) *In situ* DRIFTS spectra of CO adsorption at 50 °C. (b) Ru 3p XPS and (c) Ru L-edge NEXAFS spectra of Ru/ZrH_2 and C_{60}-Ru/ZrH_2 catalysts. (d) Kh_T calculation results from the NEXAFS spectra.

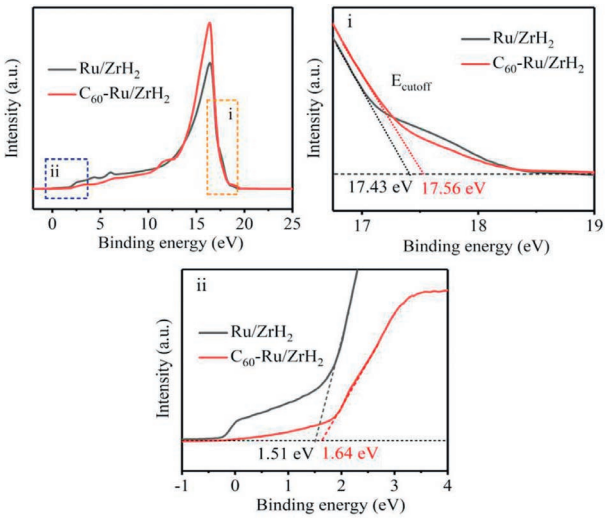


Fig. 5. UPS spectra and the magnified images of corresponding positions i and ii over Ru/ZrH_2 and C_{60}-Ru/ZrH_2 catalysts.

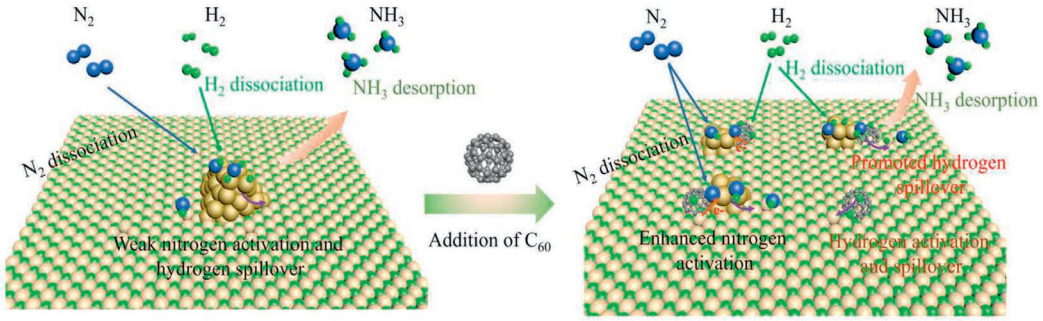
Ru/ZrH_2 can be attributed to multicarbonyl species adsorbed on oxidized Ru sites ([$Ru^{\delta+}$-$(CO)_x$]) [45,46]. Two peaks located at 2019 and 1989 cm^{-1} are attributed to the mono-adsorption of CO at the step site [12] and the bonding of CO to the Ru bridge site at the Ru-support interface [47,48], respectively. Interestingly, the intensity of the absorption peaks for C_{60}-Ru/ZrH_2 is significantly higher than that of Ru/ZrH_2. This observation indicates that the addition of C_{60} results in a significant increase in the number of exposed step and interface Ru sites, which can be attributed to the reduction in Ru particle size after C_{60} doping. Compared to Ru/ZrH_2, the disappearance of the peak at 2066 cm^{-1} and the slight redshift of the other two peaks (2012 and 1980 cm^{-1}) in the C_{60}-Ru/ZrH_2 catalyst indicate that the addition of C_{60} is favourable for stabilizing low-valence state Ru^0 species [49].

Moreover, the chemical states of the Ru species on Ru/ZrH_2 and C_{60}-Ru/ZrH_2 were investigated using X-ray photoelectron spectroscopy (XPS). The Ru 3p XPS spectrum of Ru/ZrH_2 shows two peaks at ~462.1 and 484.3 eV, corresponding to Ru $3p_{3/2}$ and Ru $3p_{1/2}$, respectively (Fig. 4b) [50]. Clearly, the Ru 3p spectrum of C_{60}-Ru/ZrH_2 is negatively shifted by 0.4 eV compared to that of Ru/ZrH_2, indicating that the Ru species in C_{60}-Ru/ZrH_2 exhibit a state of electron enrichment. Furthermore, the Ru 3p XPS spectra of these two catalysts can be further deconvoluted into multiple peaks, which can be assigned to Ru^0 and $Ru^{\delta+}$ [51]. Notably, the ratio of $Ru^0/(Ru^0+Ru^{\delta+})$ for C_{60}-Ru/ZrH_2 is 52.4 %, which is higher than the ratio for Ru/ZrH_2 at 46.7 %. This indicates that the addition of C_{60} leads to the formation of a greater number of metallic Ru sites.

To further identify the electronic structure of the Ru sites, synchrotron radiation-based near-edge X-ray absorption fine structure spectroscopy (NEXAFS) was conducted. The white lines observed at the Ru L_3- and L_2-edges in the NEXAFS primarily reflect electron transitions from the Ru core $2p_{3/2}$ and $2p_{1/2}$ to the unoccupied $4d_{5/2}$ and $4d_{3/2}$ orbitals [52,53], respectively. Therefore, the intensity of the white line can be utilized as a metric for assessing the empty state density of the Ru d orbitals or the quantity of 4d holes [54]. As shown in Fig. 4c, the C_{60}-promoted Ru/ZrH_2 catalyst exhibits a significantly lower white-line intensity compared to that of Ru/ZrH_2, indicating that more occupied states are formed in the Ru d orbitals after C_{60} doping. This phenomenon arises from the strong electronic coupling interaction between the C_{60} and Ru atoms, resulting in the formation of fewer 4d holes, which is consistent with the XPS results. The extent of electron transfer is influenced by the number of unoccupied d orbitals (Kh_T) at the Ru sites, which can be semi-quantitatively assessed using the Ru L-edge NEXAFS spectra [54]. The Kh_T value for C_{60}-Ru/ZrH_2 (0.53) is obviously lower than that of Ru/ZrH_2 (0.74) (Fig. 4d and Table S3 in Supporting information). This indicates that the introduction of C_{60} induces a strong interaction between the C_{60} π-orbitals and the Ru 4d orbitals, resulting in a substantial decrease in the amount of unpaired Ru 4d charge.

To further investigate the impact of C_{60} addition on the electronic structure of these catalysts, ultraviolet photoelectron spectroscopy (UPS) measurements were conducted (Fig. 5). The work function (Φ_{WF}), determined from the cutoff of the secondary electron emission (magnified image i), is 3.79 eV for Ru/ZrH_2 and 3.66 eV for C_{60}-Ru/ZrH_2, respectively. The doping of C_{60} decreases the work function, enabling that the trapped electrons at the C_{60}-Ru/ZrH_2 interface are loosely bound. This results in a decreased barrier for electron donation from the Ru sites to the anti-bonding π orbitals of the adsorbed N_2 [55,56]. Consequently, this weakens the N≡N bond and promotes the activation of N_2. Moreover, upon the addition of C_{60}, the d-band center (ε_d, as shown in the magnified image ii) of the Ru/ZrH_2 catalyst shifts downward from −1.51 eV to −1.64 eV with respect to the Fermi energy. This downshift in ε_d for the C_{60}-Ru/ZrH_2 indicates a decrease in the anti-bonding energy state, which results in a weakened interaction between the adsorbed intermediate species NH_x (where $x = 0$–3) and Ru metal. This weakening is beneficial for the NH_x desorption process, as evidenced by the significantly higher positive NH_3 reaction order observed with C_{60}-Ru/ZrH_2 compared to Ru/ZrH_2. These findings suggest that the introduction of C_{60} plays a crucial role in reducing the work function and lowering the d-band center of the Ru/ZrH_2 catalyst. This adjustment simultaneously meets the electronic requirements for promoting N_2 activation and facilitating NH_x desorption. This effect may be attributed to the function of C_{60} as an electron buffer, which helps balance the electron density of the active metal [27,28].

Previous studies have shown that negative hydrogen (H^-) ions in hydrides are reactive during NH_3 synthesis process [57–59]. To determine whether H^- ions in ZrH_2 can participate in the formation of NH_3, we exposed the C_{60}-Ru/ZrH_2 catalyst to pure N_2 to detect the NH_3 yield at 400 °C and 1 MPa. With the progress of the reaction time, the accumulated amount of NH_3 at the outlet gradually increased and approached a steady state after 12 h (Fig. S11



Scheme 1. Reaction pathways of Ru-based catalysts with or without C_{60} modification for NH_3 synthesis.

in Supporting information), indicating that the H^- ions in ZrH_2 can combine with the N species to form NH_3. To further investigate the reactivity of H species in C_{60}-Ru/ZrH_2, an isothermal surface reaction experiment was performed at 400 °C. As shown in Fig. S12 (Supporting information), the NH_3 signal gradually decreases with the introduction of 5 %N_2/Ar gas, indicating the depletion of H species and the subsequent formation of H vacancies. When the gas was switched to 10 %H_2/Ar, the NH_3 signal was largely restored, indicating that the H species in ZrH_2 can be replenished and react with the adsorbed N species to form NH_3. A similar isothermal surface reaction experiment was performed with isotopic D_2 to further verify that H species in the catalyst can be supplemented (Fig. S13 in Supporting information). When D_2 gas was introduced, signals for ND_3 ($m/z = 20$) and ND_2H ($m/z = 19$) were detected, revealing that the D species in the replenished C_{60}-Ru/ZrH_2 originated from gas-phase D_2 [60]. Additionally, a stronger HD ($m/z = 3$) signal is observed from the C_{60}-modified Ru/ZrH_2 catalyst compared to that from the Ru/ZrH_2 (Fig. S14 in Supporting information). This observation demonstrates that the presence of C_{60} enhances the activation of H_2 and facilitates the exchange of lattice H species with gaseous H_2. H_2-temperature programmed desorption (H_2-TPD) curve (Fig. S15 in Supporting information) for Ru/ZrH_2 shows two distinct H_2 desorption peaks: one in the range of 420–600 °C (α) and another in the range of 600–800 °C (β), corresponding to the desorption of H_2 from the Ru surface or subsurface sites and the ZrH_2 support, respectively. Notably, the introduction of C_{60} into Ru/ZrH_2 increases the intensity of the two H_2 desorption peaks and shifts these peaks to lower temperature (α peak), indicating that the presence of C_{60} enhances the spillover effect of hydrogen species while weakening the adsorption strength at the subsurface sites. Moreover, the presence of C_{60} accelerates the migration and spillover of hydrogen species, as further demonstrated by the WO_3 color change experiment [28,61]. As shown in Fig. S16 (Supporting information), pure WO_3 does not exhibit significant color changes. However, a more pronounced color change is observed in the C_{60}-modified Ru/ZrH_2 compared to the unmodified Ru/ZrH_2 during hydrogen treatment. This indicates that the addition of C_{60} enhances the migration of adsorbed hydrogen species. Moreover, the addition of C_{60} significantly increases the amount of NH_3 desorption compared to the C_{60}-free Ru sample (Fig. S17 in Supporting information). This suggests that the presence of C_{60} facilitates the formation of more active sites with weaker NH_3 adsorption, which is consistent with the remarkable increase in the NH_3 reaction order after C_{60} doping (Fig. 2d).

To elucidate the reaction pathway for NH_3 synthesis, we conducted isotope reaction experiments using a C_{60}-Ru/ZrH_2 catalyst with a feedstock gas mixture of $^{15}N_2$–$^{14}N_2$-H_2 at a temperature of 400 °C. If the dissociation of N_2 is the rate-determining step (RDS), then the dissociated nitrogen (N) atoms can immediately react with hydrogen species to form NH_3. Conversely, if the formation of N–H_x is the RDS, the dissociated N atoms may accumulate and exchange to form $^{14}N^{15}N$ species [21,42]. As shown in Fig. S18 (Supporting information), a distinct signal for $^{14}N^{15}N$ ($m/z = 29$) is observed in the C_{60}-Ru/ZrH_2 catalyst compare to that of Ru/ZrH_2, which proves the shift of RDS from the dissociation of N_2 to the formation of the N–H_x bond. This may be attributed to the lower activation energy (Fig. 2a) and the smaller reaction order for N_2 (Fig. 2b) associated with the C_{60} modification. As a result, the C_{60}-Ru/ZrH_2 catalyst can efficiently activate N_2, leading to outstanding NH_3 synthesis performance (Scheme 1).

To summarize, we developed a C_{60}-modified Ru/ZrH_2 catalyst that serves as an efficient catalyst for NH_3 synthesis at mild conditions. Our results demonstrate that the strong interaction between the C_{60} and Ru entities not only regulates the charge density of Ru atoms but also promotes the dispersion of Ru species to expose more step sites. Meanwhile, the presence of C_{60} facilitates the exchange of lattice H species in ZrH_2 with gaseous H_2 and accelerates the hydrogen spillover from Ru metal to the catalyst surface. Therefore, the NH_3 synthesis rate of the C_{60}-modified Ru/ZrH_2 catalyst is approximately 2 times as high as that of the C_{60}-free Ru sample at 400 °C and 1 MPa. This enhancement is attributed to the co-optimization of nitrogen activation and hydrogen migration resulting from the addition of C_{60}. Moreover, the incorporation of C_{60} adjusts the d-band center, facilitating the desorption of NH_3 from the catalyst surface and thereby freeing up additional active sites for the continuous activation of N_2. These findings broaden the range of promoters available for the NH_3 synthesis reaction.

Declaration of competing interest

The authors declare that they have no known competing financial interests or personal relationships that could have appeared to influence the work reported in this paper.

CRediT authorship contribution statement

Xuanbei Peng: Writing – review & editing, Writing – original draft, Investigation, Formal analysis. **Xiaohu Hu:** Validation, Investigation, Formal analysis. **Ruishao Mao:** Validation, Investigation, Formal analysis. **Mengqi An:** Investigation. **Jiaxin Li:** Investigation. **Yangyu Zhang:** Investigation. **Tianhua Zhang:** Investigation. **Ming Chen:** Investigation. **Yanliang Zhou:** Writing – review & editing. **Jun Ni:** Supervision, Resources, Investigation. **Lirong Zheng:** Resources. **Xiuyun Wang:** Writing – review & editing, Supervision, Resources, Funding acquisition. **Lilong Jiang:** Supervision, Resources, Project administration, Funding acquisition.

Acknowledgments

The work was supported by the National Key Research and Development Program (No. 2022YFA1604101), and National Natural Science Foundation of China (Nos. 22222801, 22221005,

92361303, 22038002, 22478075, 22472028, 22108037), and the Key R&D plan of Shanghai Science and Technology Commission (No. 21DZ1209002), and the China Postdoctoral Science Foundation (No. 2025T180317).

Supplementary materials

Supplementary material associated with this article can be found, in the online version, at doi:10.1016/j.cclet.2025.111820.

References

[1] J.G. Chen, R.M. Crooks, L.C. Seefeldt, et al., Science 360 (2018) eaar6611.
[2] B. Dutta, C. Wildfire, D. Shekhawat, Chem. Eng. J. 494 (2024) 152924.
[3] J. Guo, P. Chen, Chem 3 (2017) 709–712.
[4] A. Klerke, C.H. Christensen, J.K. Nørskov, et al., J. Mater. Chem. 18 (2008) 2304–2310.
[5] T. He, P. Pachfule, H. Wu, et al., Nat. Rev. Mater. 1 (2016) 1–17.
[6] K. Sato, S.-i. Miyahara, Y. Ogura, et al., ACS Sustain. Chem. Eng. 8 (2020) 2726–2734.
[7] T. Kandemir, M.E. Schuster, A. Senyshyn, et al., Angew. Chem. Int. Ed. 52 (2013) 12723–12726.
[8] X. Yu, B. Lin, J. Lin, et al., J. Rare Earth. 26 (2008) 711–716.
[9] L. Wang, M. Xia, H. Wang, et al., Joule 2 (2018) 1055–1074.
[10] G. Ertl, Catal. Rev. 21 (1980) 201–223.
[11] R. Zhang, C. Li, H. Cui, et al., Nat. Commun. 14 (2023) 8036.
[12] J. Zheng, F. Liao, S. Wu, et al., Angew. Chem. Int. Ed. 58 (2019) 17335–17341.
[13] C. Smith, A.K. Hill, L. Torrente-Murciano, Energ. Environ. Sci. 13 (2020) 331–344.
[14] G. Ertl, Angew. Chem. Int. Ed. 47 (2008) 3524–3535.
[15] M. Kitano, Y. Inoue, Y. Yamazaki, et al., Nat. Chem. 4 (2012) 934–940.
[16] T. Ye, S. Park, Y. Lu, et al., Nature 583 (2020) 391–395.
[17] T.N. Ye, S.W. Park, Y. Lu, et al., J. Am. Chem. Soc. 142 (2020) 14374–14383.
[18] Z. Sun, K. Li, S. Toan, et al., Chem. Eng. J. 476 (2023) 146643.
[19] P. Wang, F. Chang, W. Gao, et al., Nat. Chem. 9 (2017) 64–70.
[20] Y. Guan, W. Zhang, Q. Wang, et al., Chem. Catal. 1 (2021) 1042–1054.
[21] M. Kitano, J. Kujirai, K. Ogasawara, et al., J. Am. Chem. Soc. 141 (2019) 20344–20353.
[22] Y. Gong, H. Li, J. Wu, et al., J. Am. Chem. Soc. 144 (2022) 8683–8692.
[23] Y. Zhou, X. Peng, T. Zhang, et al., ACS Catal. 12 (2022) 7633–7642.
[24] S.E. Siporin, R.J. Davis, J. Catal. 225 (2004) 359–368.
[25] J.A. Almquist, E.D. Crittenden, Ind. Eng. Chem. 18 (1926) 1307–1309.
[26] K.I. Aika, T. Takano, S. Murata, J. Catal. 136 (1992) 126–140.
[27] J. Zheng, L. Huang, C.H. Cui, et al., Science 376 (2022) 288–292.
[28] Y. Zhang, X. Peng, H.R. Tian, et al., Nat. Chem. (2024) 1781–1787.
[29] Y. Zhang, Y. Zhou, X. Peng, et al., AIChE J. 71 (2025) e18789.
[30] X.Z. Wu, Y.R. Yao, M.M. Chen, et al., J. Am. Chem. Soc. 138 (2016) 9629–9633.
[31] J.Z. Qiu, J. Hu, J. Lan, et al., Chem. Mater. 31 (2019) 9413–9421.
[32] Y. Baik, M. Kwen, K. Lee, et al., J. Am. Chem. Soc. 145 (2023) 11364–11374.
[33] O.S. Morozova, Global Atmospheric Change and Its Impact on Regional air Quality, in: I. Barnes (Ed.), Hydrogen technology: H_2 Storage and Release, Springer, 2002, pp. 303–308.
[34] Y.J. Choi, Y. Xu, W.J. Shaw, et al., J. Phys. Chem. C 116 (2012) 8349–8358.
[35] B. Fang, C. Zhang, Z. Qi, et al., AIChE J. 68 (2022) e17849.
[36] R.D. Johnson, G. Meijer, D.S. Bethune, J. Am. Chem. Soc. 112 (1990) 8983–8984.
[37] J.D. Fortner, D.I. Kim, A.M. Boyd, et al., Environ. Sci. Technol. 41 (2007) 7497–7502.
[38] D. Saha, S. Deng, Langmuir 27 (2011) 6780–6786.
[39] A.V. Talyzin, U. Jansson, Thin Solid Films 429 (2003) 96–101.
[40] F. Leng, I.C. Gerber, P. Lecante, et al., ACS Catal. 6 (2016) 6018–6024.
[41] T. Wang, L.Y. Li, L.N. Chen, et al., J. Am. Chem. Soc. 144 (2022) 9292–9301.
[42] Y. Zhou, C.Q. Xu, Z. Tan, et al., ACS Catal. 12 (2022) 2651–2660.
[43] L.N. Zhang, Z.L. Lang, Y.H. Wang, et al., Energ. Environ. Sci. 12 (2019) 2569–2580.
[44] K. Honkala, A. Hellman, I.N. Remediakis, et al., Science 307 (2005) 555–558.
[45] W. Raróg-Pilecka, E. Miśkiewicz, D. Szmigiel, et al., J. Catal. 231 (2005) 11–19.
[46] X. Peng, X. Chen, Y. Zhou, et al., J. Catal. 408 (2022) 98–108.
[47] H.T. Chen, J. Phys. Chem. C 116 (2012) 6239–6246.
[48] B. Teng, C. Ma, J. Chen, et al., ACS Appl. Nano Mater. 7 (2024) 15012–15024.
[49] J. Li, Z. Liu, D.A. Cullen, et al., ACS Catal. 9 (2019) 11088–11103.
[50] D. Cao, J. Wang, H. Xu, et al., Small 17 (2021) 2101163.
[51] M. Tang, S. Mao, M. Li, et al., ACS Catal. 5 (2015) 3100–3107.
[52] I.C. Stefan, Y. Mo, M.R. Antonio, et al., J. Phys. Chem. B 106 (2002) 12373–12375.
[53] Y. Wen, P. Chen, L. Wang, et al., J. Am. Chem. Soc. 143 (2021) 6482–6490.
[54] D.H. Pearson, C.C. Ahn, B. Fultz, Phys. Rev. B 47 (1993) 8471.
[55] M. Xiao, L. Gao, Y. Wang, et al., J. Am. Chem. Soc. 141 (2019) 19800–19806.
[56] Y. Lu, J. Li, T. Tada, et al., J. Am. Chem. Soc. 138 (2016) 3970–3973.
[57] W. Gao, P. Wang, J. Guo, et al., ACS Catal. 7 (2017) 3654–3661.
[58] Y. Guan, C. Liu, Q. Wang, et al., Angew. Chem. Int. Ed. 61 (2022) e202205805.
[59] F. Chang, Y. Guan, X. Chang, et al., J. Am. Chem. Soc. 140 (2018) 14799–14806.
[60] L. Li, T. Zhang, J. Cai, et al., J. Catal. 389 (2020) 218–228.
[61] M. Xiong, Z. Gao, P. Zhao, et al., Nat. Commun. 11 (2020) 4773.